A&A 535, A88 (2011)
DOI: 10.1051/0004-6361/201117491

Astronomy & Astrophysics

Spectral line polarization with angle-dependent partial frequency redistribution

IV. Scattering expansion method for the Hanle effect

K. N. Nagendra and M. Sampoorna

Indian Institute of Astrophysics, Koramangala, 560 034 Bangalore, India
e-mail: sampoorna@iiap.res.in

Received 16 June 2011 / Accepted 9 September 2011

ABSTRACT

Context. The partial frequency redistribution (PRD) effects in line scattering are necessary ingredients for interpreting the linear polarization observed in strong resonance lines. It is a common practice to use angle-averaged PRD functions for simplicity (obtained by averaging over all scattering angles). It has been established that the use of angle-dependent PRD functions instead of angle-averaged functions is essential for weak fields.

Aims. Here we present an efficient iterative method to solve the polarized line radiative transfer equation in weak magnetic fields using angle-dependent PRD functions.

Methods. Based on the theory of Stokes vector decomposition for the Hanle effect combined with the Fourier azimuthal expansion of the angle-dependent PRD function, we try to formulate an efficient numerical method of solving the concerned transfer problem in one-dimensional media. This iterative method (referred to as the scattering expansion method, SEM) is based on a series expansion of the polarized source vector in mean number of scatterings (Neumann series expansion). We apply the SEM approach to handle both the exact and various approximate forms of the Hanle scattering redistribution matrix.

Results. The SEM is shown to be an efficient method to solve angle-dependent PRD problems involving the Hanle effect. We show that compared to the earlier methods such as the perturbation methods, the SEM is stable and faster. We find that angle-dependent PRD significantly affects the Stokes U parameter.

Key words. methods: numerical – polarization – magnetic fields – Sun: atmosphere – line: formation – scattering

1. Introduction

The resonance scattering is responsible for the generation of a linearly polarized solar spectrum (called the second solar spectrum). The magnetic field modifies this linear polarization through the well-known Hanle effect. The shape of the linear polarization profiles of the spectral lines reveals a great deal of information about the anisotropy that prevails in the solar atmosphere. Equally important is the physics of line scattering – namely the details of the frequency redistribution during scattering. It is well-known that for a finer analysis of the polarized spectrum, particularly of the strong resonance lines, the angle-dependent partial frequency redistribution (PRD) is necessary, as shown in the previous papers of this series (Frisch 2010; Sampoorna et al. 2011; Sampoorna 2011b).

The papers mentioned above used a decomposition technique to reduce the non-axisymmetric Stokes transfer equation to a set of six irreducible components I^K_Q, where $K = 0, 2$ and $Q \in [-K, +K]$. This is achieved through a irreducible spherical tensor expansion of the Hanle phase matrix (see Landi Degl'Innocenti & Landolfi 2004; Frisch 2007). When the PRD function used in the transfer equation is an "angle-averaged function", I^K_Q are cylindrically symmetric. However, when the PRD function is explicitly angle-dependent, the I^K_Q are non-axisymmetric. Frisch (2009) has shown that cylindrical symmetry can be retained by Fourier-expanding the angle-dependent PRD function over the azimuth angle difference $(\chi - \chi')$, where χ and χ' are the azimuth angles of the outgoing and incoming rays in the atmospheric co-ordinate system (see Fig. 1). The Fourier azimuthal expansion of the angle-dependent PRD functions was originally introduced by Domke & Hubeny (1988). This expansion was cleverly used by Frisch (2009) for the Hanle-scattering PRD transfer problem. The Fourier expansion of the angle-dependent PRD function was applied to the non-magnetic (Rayleigh scattering) problem in Frisch (2010). In this non-magnetic case there are only four cylindrically symmetric components. The relevant polarized transfer problem was solved in Sampoorna et al. (2011). Recently, Anusha & Nagendra (2011) have generalized to the case of multi-dimensional media, the Fourier decomposition technique of Frisch (2009) originally formulated for the one-dimensional case.

An approximate solution (namely, single scattering approximation) to the Hanle transfer problem with angle-dependent PRD was presented in Sampoorna (2011b). Here we solve the full Hanle transfer problem in one-dimensional media by applying the scattering expansion method (SEM). This method was originally formulated by Frisch et al. (2009) for solving the polarized line transfer equation with complete frequency redistribution (CRD). Subsequently it has been generalized by Sampoorna et al. (2011) to solve the polarized Rayleigh scattering transfer equation with angle-dependent PRD.

A detailed historical account of the work on angle-dependent PRD in polarized line transfer is given in Sampoorna et al. (2011). We refer to the same paper for references about early works on transforming the transfer equation from the Stokes vector (I, Q, U) basis to the cylindrically symmetric irreducible basis.

The organization of the paper is as follows. In Sect. 2 we recall the exact and various approximate forms of the Hanle scattering redistribution matrix. In Sect. 3 we briefly recall the decomposition technique of Frisch (2009), but suitably generalized here to accommodate the different forms of the Hanle scattering redistribution matrices discussed in Sect. 2. In Sect. 4 we present the equations of the SEM to solve the relevant transfer problems. The exact form of the Hanle scattering redistribution matrix discussed in Sect. 2 is included in the decomposition technique of Frisch (2009) in Sect. 3. It involves the azimuthal Fourier coefficients on the order of 0, 1, 2, 3, and 4 of the magnetic redistribution functions (see Sampoorna et al. 2007a,b). In Sect. 5 we discuss the properties of these functions. Section 6 is devoted to the results, and the conclusions are given in Sect. 7. An erratum is given in Sect. 8. In Appendix A we present the composite redistribution functions that enter the exact form of the Hanle scattering redistribution matrix. Appendix B contains a listing of the azimuthal Fourier coefficients.

2. Redistribution matrix for the weak-field Hanle scattering

In early works on scattering of radiation on atoms the problem of the frequency redistribution was ignored. For example, the Rayleigh phase matrix for resonance scattering in the absence of magnetic fields was derived by Hamilton (1947, see also Chandrasekhar 1950). In the presence of weak magnetic fields the expression for the Hanle phase matrix was derived by Stenflo (1978) and Landi Degl'Innocenti & Landi Degl'Innocenti (1988).

The problem of frequency redistribution during scattering in the presence of a weak magnetic field and collisions was originally addressed by Omont et al. (1973). However, they did not present the explicit form of the Hanle scattering redistribution matrix. But they remarked that the Hanle effect is operative only in the line core and not in the line wings. Owing to the very short life-time of the excited level in the wing frequencies, the Hanle effect cannot effectively intervene during the scattering process. On the basis of these results, a heuristic (in the sense that we presume a decoupling of frequency redistribution function, and the angular phase matrix) form for the elements of the Hanle redistribution matrix in the presence of a weak magnetic field $\boldsymbol{B}$ can be written as

$$\hat{R}_{ij}(x, \boldsymbol{\Omega}, x', \boldsymbol{\Omega}', \boldsymbol{B}) = R(x, x', \Theta)\hat{P}_{ij}(\boldsymbol{\Omega}, \boldsymbol{\Omega}', \boldsymbol{B}), \tag{1}$$

where $i, j = 0, 1, 2$. $R(x, x', \Theta)$ stands for any of the type I, II, or III PRD functions of Hummer (1962), and Θ is the angle between the incoming ($\boldsymbol{\Omega}'$) and outgoing ($\boldsymbol{\Omega}$) rays (see Fig. 1). x and x' are outgoing and incoming frequencies in Doppler width units. $\hat{P}_{ij}(\boldsymbol{\Omega}, \boldsymbol{\Omega}', \boldsymbol{B})$ are the elements of the Hanle phase matrix (see Stenflo 1978; Landi Degl'Innocenti & Landi Degl'Innocenti 1988). Equation (1) is valid only in the line core, namely $x \le x_c$, where x_c denotes the transition frequency between line core and the wings. For $x > x_c$, redistribution matrix is given by Eq. (1) itself but with the Rayleigh phase matrix replacing the Hanle phase matrix. We refer to this division into Hanle and Rayleigh frequency domains as 1D cut-off approximation and x_c as 1D cut-off frequency – generally taken to be three Doppler widths. This approximation but with the angle-averaged redistribution function $R(x, x')$ in Eq. (1) instead of $R(x, x', \Theta)$ was used in several previous works (see e.g., Faurobert-Scholl 1992; Nagendra et al. 1999).

A general PRD matrix that takes into account the effects of elastic collisions in the presence of arbitrary magnetic fields was derived by Bommier (1997). In the weak-field limit (Zeeman splitting of the upper level much smaller than the Doppler width of the line), the coupling of circular polarization to the linear polarization and also to the intensity is weak and can be neglected. The resulting Hanle scattering redistribution matrix is exact in the sense that it does not make use of the frequency domains to represent the transition from Hanle scattering in the line core to the Rayleigh scattering in the line wings. Bommier (1997) refers to it as approximation I, because it is derived only under the "weak-field limit". Indeed, in approximation I the coupling of frequency redistribution to the linear polarization is kept intact. The angle-averaged version of this approximation I was used in polarized line transfer computations by Sampoorna et al. (2008).

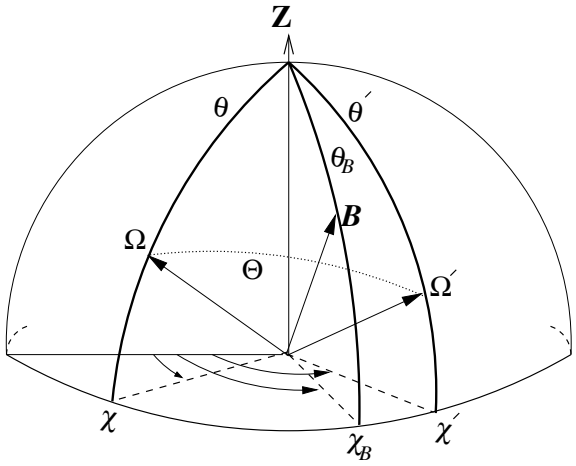

Fig. 1. Geometry showing the scattering process in the atmospheric co-ordinate system (Z-axis along the atmospheric normal). The magnetic field makes an angle θ_B with respect to the polar Z-axis, and has an azimuth χ_B. (θ', χ') refer to the incident ray, and (θ, χ) to the scattered ray defined with respect to the polar Z-axis. Θ is the scattering angle.

In the present paper we confine our attention only to pure type-II scattering. Thus in the absence of elastic collisions, the angle-dependent redistribution matrix under approximation I may be written as (see Bommier 1997)

$$\hat{R}_{ij}(x, \boldsymbol{\Omega}, x', \boldsymbol{\Omega}', \boldsymbol{B}) = \sum_{KQQ'} \mathcal{T}^K_Q(i, \boldsymbol{\Omega})\mathcal{N}^K_{QQ'}(x, x', \Theta, \boldsymbol{B})(-1)^{Q'}\mathcal{T}^K_{-Q'}(j, \boldsymbol{\Omega}'). \tag{2}$$

Here $\mathcal{T}^K_Q(i, \boldsymbol{\Omega})$ are irreducible spherical tensors introduced by Landi Degl'Innocenti (1984). The magnetic kernel is of the form

$$\mathcal{N}^K_{QQ'}(x, x', \Theta, \boldsymbol{B}) = \mathrm{e}^{\mathrm{i}(Q'-Q)\chi_B} \sum_{Q''} d^K_{QQ''}(\theta_B) d^K_{Q''Q'}(-\theta_B) \times Z^{\mathrm{II}}_{KQ''}(x, x', \Theta, B). \tag{3}$$

Here θ_B and χ_B represent the orientation of the magnetic field in the atmospheric co-ordinate system (see Fig. 1). Explicit expressions for the reduced rotation matrices $d^K_{QQ'}$ can be found in Landi Degl'Innocenti & Landolfi (2004, Table 2.1, p. 57). For a two-level atom with an unpolarized lower level and a $J \to J' \to J$ scattering transition (where J and J' are the total angular momentum quantum numbers of lower and upper levels, respectively), Z^{II}_{KQ} takes the form

$$Z^{\mathrm{II}}_{KQ}(x, x', \Theta, B) = \frac{\Gamma_{\mathrm{R}}}{\Gamma_{\mathrm{R}} + \Gamma_{\mathrm{I}} + \mathrm{i}\omega_{\mathrm{L}} g_{J'} Q} \times w^{(K)}_{J'J} \mathcal{R}^{K,K}_{Q,\mathrm{II}}(x, x', \Theta, B), \tag{4}$$

where Γ_R is the radiative de-excitation rate, Γ_I is the inelastic collisional de-excitation rate, ω_L is the Larmor frequency, and $g_{J'}$ is the Landé factor of the upper level. The quantities $w^{(K)}_{J'J}$ are defined in Eq. (10.11) of Landi Degl'Innocenti & Landolfi (2004). The composite redistribution functions of type-II ($\mathcal{R}^{K,K}_{Q,\mathrm{II}}$) are linear combinations of angle-dependent magnetic redistribution functions of type-II (see Sampoorna et al. 2007a,b, also Sampoorna 2011a). The explicit form of these functions for a $J = 0 \to 1 \to 0$ scattering transition can be found in Appendix A of Sampoorna et al. (2007b). For an arbitrary $J \to J' \to J$ scattering transition the $\mathcal{R}^{K,K}_{Q,\mathrm{II}}$ are given in Appendix A of the present paper.

For practical applications, Bommier (1997) also derived the so-called approximations II and III, where the 2D frequency space (x, x') is decomposed into several domains, in each of which the frequency redistribution is "decoupled" from the polarization. Approximation II uses the angle-dependent PRD functions, and approximation III the corresponding angle-averaged functions of Hummer (1962). The approximations II and III for the Hanle redistribution matrix have been considered in Nagendra et al. (2002, see also Nagendra et al. 2003), where a perturbation method is used to solve the concerned polarized transfer equation. For approximation III a polarized accelerated lambda iteration (ALI) method based on the core-wing approach was later developed by Fluri et al. (2003).

Under approximation II and in the absence of elastic collisions, the redistribution matrix is given by Eq. (2), but with the replacement

$$\mathcal{N}^K_{QQ'}(x, x', \Theta, \boldsymbol{B}) = \mathcal{N}^K_{QQ'}(m, \boldsymbol{B}) R_{\mathrm{II}}(x, x', \Theta). \tag{5}$$

Here the index m (=1, 2) stands for different (x, x') frequency domains. Under approximation III the redistribution matrix is given by Eqs. (2) and (5), but with the angle-dependent redistribution function replaced by the angle-averaged one. The analytic form of the magnetic kernels $\mathcal{N}^K_{QQ'}(m, \boldsymbol{B})$ in different angle-dependent (approximation II) and angle-averaged (approximation III) frequency domains can be found in Bommier (1997, see also Nagendra et al. 2002; Anusha et al. 2011). It is useful to note that in approximations II and III there is a factorization of frequency redistribution and polarization, so that $\mathcal{N}^K_{QQ'}(m, \boldsymbol{B})$ within a given domain depends only on $\boldsymbol{B}$, unlike in approximation I which is a non-domain-based theory.

In the 1D cut-off approximation, $\mathcal{N}^K_{QQ'}$ takes the form

$$\mathcal{N}^K_{QQ'}(x, x', \Theta, \boldsymbol{B}) = R(x, x', \Theta) \times \begin{cases} \mathcal{N}^K_{QQ'}(\boldsymbol{B}), & \text{for} \quad x \le x_c, \\ (1-\epsilon) W_K \delta_{QQ'}, & \text{for} \quad x > x_c, \end{cases} \tag{6}$$

where W_K is the polarizability factor depending on the J-quantum numbers of the upper and lower levels, and ϵ is the thermalization parameter.

3. A decomposition method for Hanle effect with angle-dependent PRD

Here we describe the Stokes vector decomposition method, which enables us to write the original "Stokes vector transfer equation" in a simplified form. The simplification takes place because the "decomposed (irreducible) transfer equation" becomes azimuth-angle-independent. In fact, this irreducible transfer equation for the cylindrically symmetric Fourier components of the radiation field allows us to formulate an iterative method of solution. Here we present only the essential steps of this decomposition technique. The full details are given in Frisch (2009).

The polarized transfer equation for the Stokes vector can be written in the component form as

$$\mu \frac{\partial I_i}{\partial \tau} = [\varphi(x) + r]\,[I_i(\tau, x, \boldsymbol{\Omega}) - S_i(\tau, x, \boldsymbol{\Omega})], \quad i = 0, 1, 2, \tag{7}$$

where $\boldsymbol{\Omega}$ (θ, χ) is the ray direction with respect to the atmospheric normal (see Fig. 1) and $\mu = \cos\theta$. The line optical depth is denoted by τ and $\varphi(x)$ is the normalized Voigt function. The ratio of continuum to line absorption coefficient is denoted by r. The total source vector is given by

$$S_i(\tau, x, \boldsymbol{\Omega}) = \frac{\varphi(x) S_{1,i}(\tau, x, \boldsymbol{\Omega}) + r S_{c,i}}{\varphi(x) + r}, \tag{8}$$

where $S_{c,i}$ are the components of the unpolarized continuum source vector. We assume that $S_{c,0} = B_{\nu_0}$, where B_{ν_0} is the Planck function at the line center, and $S_{c,1} = S_{c,2} = 0$. The line source vector can be written as

$$S_{1,i}(\tau, x, \boldsymbol{\Omega}) = G_i(\tau) + \int \oint \sum_{j=0}^{2} \frac{\hat{R}_{ij}(x, \boldsymbol{\Omega}, x', \boldsymbol{\Omega}', \boldsymbol{B})}{\varphi(x)} I_j(\tau, x', \boldsymbol{\Omega}') \frac{\mathrm{d}\Omega'}{4\pi}\, \mathrm{d}x', \tag{9}$$

where $\boldsymbol{\Omega}'$ (θ', χ') is the direction of the incoming ray defined with respect to the atmospheric normal, and $\mathrm{d}\Omega' = \sin\theta'\, \mathrm{d}\theta'\, \mathrm{d}\chi'$. The primary source is assumed to be unpolarized, so that $G_0(\tau) = \epsilon B_{\nu_0}$ and $G_1(\tau) = G_2(\tau) = 0$.

Frisch (2009) has shown that the Stokes vector and the source vector can be decomposed into six irreducible components I^K_Q and S^K_Q. However, these components continue to be non-axisymmetric because of the presence of an angle-dependent PRD function. The problem can be simplified only through the introduction of an azimuthal Fourier expansion of the angle-dependent PRD function. Using this approach the I^K_Q can also be expanded over the azimuth χ as

$$I^K_Q(\tau, x, \boldsymbol{\Omega}) = \frac{1}{2} \sum_{k=-\infty}^{k=+\infty} \tilde{I}^{(k)K}_Q(\tau, x, \theta) \mathrm{e}^{\mathrm{i}k\chi}, \tag{10}$$

with similar expansions for G^K_Q and S^K_Q (see Frisch 2009, for details). The Fourier coefficients $\tilde{I}^{(k)K}_Q$ satisfy a non-LTE transfer equation similar to Eq. (7), with the source term given by Eq. (8), but with $\tilde{S}^{(k)K}_{1,Q}$ and $\tilde{S}^{(k)K}_{c,Q}$ instead of $S_{1,i}$ and $S_{c,i}$. Because the continuum is assumed to be unpolarized, $\tilde{S}^{(k)K}_{c,Q} = 2\delta_{0k}\delta_{0K}\delta_{0Q} B_{\nu_0}$. The Fourier coefficients of the line source vector are given by

$$\tilde{S}^{(k)K}_{1,Q}(\tau, x, \theta) = \tilde{G}^{(k)K}_Q(\tau) + \sum_{Q'} \frac{1}{2} \int_{-\infty}^{+\infty} \int_0^{\pi} \times \frac{\tilde{\mathcal{N}}^{(k)K}_{QQ'}(x, \theta, x', \theta', \boldsymbol{B})}{\varphi(x)} \sum_{K'Q''} \frac{1}{2} \tilde{\Gamma}^{(k-k')}_{KQ',K'Q''}(\theta') \times \tilde{I}^{(k')K'}_{Q''}(\tau, x', \theta') \sin\theta'\, \mathrm{d}\theta'\, \mathrm{d}x', \tag{11}$$

where the primary source term $\tilde{G}^{(k)K}_Q(\tau) = 2\delta_{0k}\delta_{0K}\delta_{0Q} G_0(\tau)$, and k and k' together satisfy the condition $k' = k + Q' - Q''$. From this condition, it follows that for a given value of k, the

values of k' get restricted to $k-4 \le k' \le k+4$. The non-zero azimuthal Fourier coefficients are of the form

$$\tilde{\Gamma}^{(Q''-Q')}_{KQ',K'Q''}(\theta') = \sum_{i=0}^{2}(-1)^{Q'}\tilde{\mathcal{T}}^{K}_{-Q'}(i,\theta')\tilde{\mathcal{T}}^{K'}_{Q''}(i,\theta'), \tag{12}$$

with K and K' both even or both odd. $\tilde{\mathcal{T}}^{K}_{Q}(i,\theta)$ are a combination of trigonometric functions, and are given by $\mathcal{T}^{K}_{Q}(i,\boldsymbol{\Omega}) = \tilde{\mathcal{T}}^{K}_{Q}(i,\theta)\mathrm{e}^{\mathrm{i}Q\chi}$. The analytic form of the magnetic kernel in the Fourier basis $\tilde{\mathcal{N}}^{(k)K}_{QQ'}$ depends on the level of approximation used to represent the Hanle redistribution matrix (see Sect. 2 for details). Below we present the form of $\tilde{\mathcal{N}}^{(k)K}_{QQ'}$ for different choices of approximation levels (1D cut-off, approximations II and I of Bommier 1997).

In the 1D cut-off approximation

$$\tilde{\mathcal{N}}^{(k)K}_{QQ'}(x,\theta,x',\theta',\boldsymbol{B}) = \tilde{r}^{(k)}(x,\theta,x',\theta') \times \begin{cases} \mathcal{N}^{K}_{QQ'}(\boldsymbol{B}), & \text{for} \quad x \le x_{\mathrm{c}}, \\ (1-\epsilon)W_K\delta_{QQ'}, & \text{for} \quad x > x_{\mathrm{c}}. \end{cases} \tag{13}$$

The Fourier coefficients $\tilde{r}^{(k)}$ of the angle-dependent PRD function are given by Eq. (14) of Frisch (2009, see also Eq. (8) of Sampoorna 2011b).

The difficulty in implementing the approximation II in the decomposition method given above was discussed in Sampoorna (2011b). Basically the domains of approximation II depend on both the frequencies (x, x') and the scattering angle Θ, while we work in the Fourier basis which is inherently azimuth-angle independent. To handle this difficulty, Sampoorna (2011b) used the angle-averaged frequency domains of approximation III, but continued to use the angle-dependent PRD functions of Hummer (1962). With this simplification $\tilde{\mathcal{N}}^{(k)K}_{QQ'}$ for approximation II is given by

$$\tilde{\mathcal{N}}^{(k)K}_{QQ'}(x,\theta,x',\theta',\boldsymbol{B}) = \mathcal{N}^{K}_{QQ'}(m,\boldsymbol{B})\tilde{r}^{(k)}_{\mathrm{II}}(x,\theta,x',\theta'). \tag{14}$$

For approximation I (non-domain-based PRD theory) the $\tilde{\mathcal{N}}^{(k)K}_{QQ'}$ is given by Eqs. (3) and (4), but with $\mathcal{R}^{K,K}_{Q,\mathrm{II}}$ replaced by $\tilde{\mathcal{R}}^{(k)K,K}_{Q,\mathrm{II}}$. In this case, the Fourier azimuthal expansion is applied to the 'magnetic redistribution functions' instead of the Hummer's PRD functions.

Notice that the range of k values extend a priori from $-\infty$ to $+\infty$, which produces an infinite set of integral equations for $\tilde{S}^{(k)K}_{1,Q}(\tau,x,\theta)$. A numerical solution is possible only if we truncate this infinite set. In practice the number of Fourier coefficients required is determined by the number of terms needed to accurately represent the angle-dependent PRD function. For the type-II PRD function of Hummer (1962), Domke & Hubeny (1988) have shown that at least five terms are needed to represent the exact value of the function to a sufficient accuracy. Thus for $k = 0, \pm1, \pm2, \pm3, \pm4$, we obtain a set of 54 coupled integral equations. In the following section we present an iterative method called the SEM to solve Eq. (11) efficiently (see Frisch et al. 2009; Sampoorna et al. 2011).

4. Scattering expansion method for Hanle effect with angle-dependent PRD

Here we present an iterative method based on a Neumann series expansion of the components of the source vector contributing to the polarization. This iterative method was referred to as SEM by Sampoorna et al. (2011), who applied it to the non-magnetic polarized line transfer problem with angle-dependent PRD. Indeed, these authors showed that this method is faster than the core-wing-based polarized ALI method.

The Neumann series amounts to an expansion in terms of the mean number of scattering events (see Frisch et al. 2009). Its first term yields the so-called "single scattered solution". For Rayleigh scattering with angle-dependent PRD the single scattering approximation to the polarized source vector components was presented by Frisch (2010). For the Hanle effect with angle-dependent PRD the corresponding approximation was presented recently by Sampoorna (2011b). The inclusion of higher-order terms in the Neumann series allows us to include multiple scattering effects in the expression for the polarized source vector components.

We first neglect polarization in the calculation of Stokes I, i.e., we assume that Stokes I is cylindrically symmetric and is given by the component $\tilde{I}^{(0)0}_{0}$ itself to an excellent approximation. This component is the solution of a non-LTE unpolarized radiative transfer equation with the line source vector given by

$$S^{0}_{1,0}(\tau,x,\theta) = \epsilon B_{\nu_0} + (1-\epsilon) \times \frac{1}{2}\int_{-\infty}^{+\infty}\int_{0}^{\pi}\frac{r^{(0)}(x,\theta,x',\theta')}{\varphi(x)}I^{0}_{0}(\tau,x',\theta')\sin\theta'\,\mathrm{d}\theta'\,\mathrm{d}x', \tag{15}$$

where $r^{(0)} = \tilde{r}^{(0)}/2$, $I^{0}_{0} = \tilde{I}^{(0)0}_{0}/2$, and $S^{0}_{1,0} = \tilde{S}^{(0)0}_{1,0}/2$. Equation (15) can be solved using a scalar ALI method based on a core-wing approach. Keeping only the contribution of $\tilde{I}^{(0)0}_{0}$ on the RHS of Eq. (11) to the $K = 2$ Fourier coefficients, we can show that values of k are limited to $k = 0, \pm1$, and ±2 (see Sampoorna 2011b). Thus the single scattering approximation for each component $\tilde{S}^{(k)2}_{1,Q}$ can be written as

$$\left[\tilde{S}^{(k)2}_{1,Q}(\tau,x,\theta)\right]^{(1)} \simeq \frac{1}{2}\int_{-\infty}^{+\infty}\int_{0}^{\pi}\frac{\tilde{\mathcal{N}}^{(k)2}_{Q-k}(x,\theta,x',\theta',\boldsymbol{B})}{\varphi(x)} \times \tilde{\Gamma}^{(k)}_{2-k,00}(\theta')I^{0}_{0}(\tau,x',\theta')\sin\theta'\,\mathrm{d}\theta'\,\mathrm{d}x'. \tag{16}$$

The superscript 1 stands for the single scattering approximation to the polarized component of the source vector. The corresponding radiation field $\left[\tilde{I}^{(k)2}_{Q}\right]^{(1)}$ for $k = 0, \pm1, \pm2$ is calculated with a formal solver and it serves as a starting solution for calculating the higher-order terms.

The higher-order terms can be obtained by substituting for $\tilde{I}^{(k')K'}_{Q''}$ appearing in the RHS of Eq. (11), from $\left[\tilde{I}^{(0)K'}_{Q''}\right]^{(1)}$. Clearly, as in the single scattering approximation, we continue to set $k' = 0$, but include the coupling of $(K = 2, Q)$ components with other polarization components $(K' = 2, Q'')$ that were neglected in the single scattering approximation. However, we neglect the coupling of the Fourier components k with other $k' \neq 0$ Fourier components, even-though $k' = \pm1$ and ±2 Fourier components are available from the single scattered solution. The advantage of retaining only the $k' = 0$ term in the RHS of Eq. (11) is that the value of k, which is now decided by the condition $k = Q'' - Q'$, is now limited to 0, ±1, ±2, ±3, and ±4. In other words, only four more values of k are needed to account for higher-order terms compared to the single scattering approximation. Consequently, the inclusion of higher-order terms increases the number of the $K = 2$ Fourier coefficients that contribute to the source vector from 25 for single scattering to 45 for higher orders of scattering. We have verified that retaining the coupling of k with, say, $k' = \pm1$ Fourier components does not lead to significant

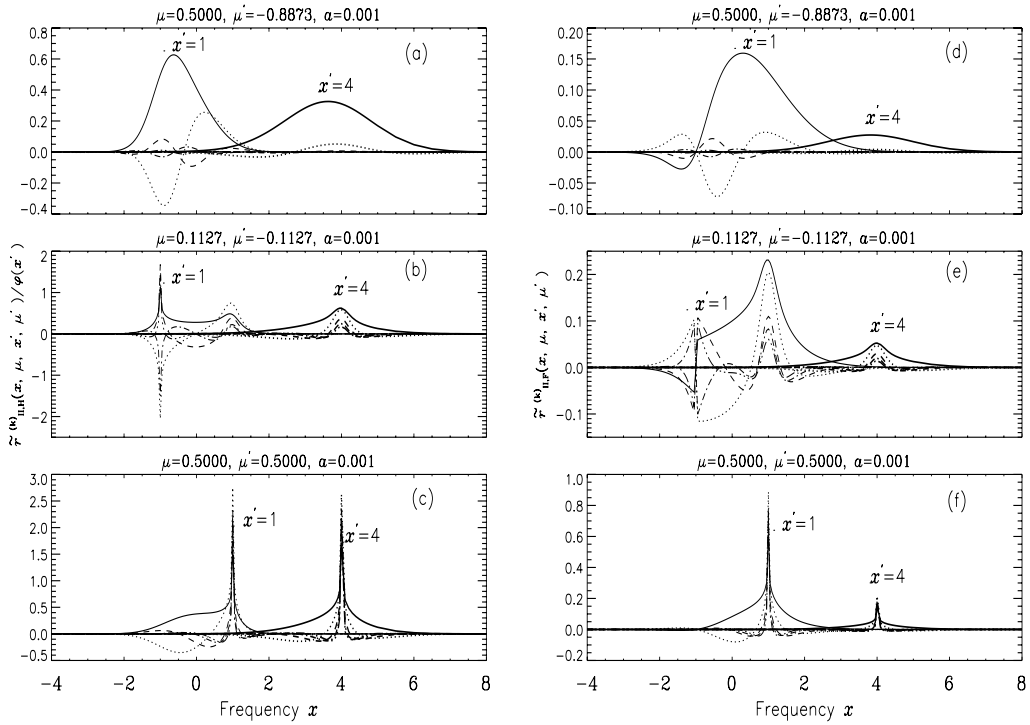

Fig. 2. Azimuthal Fourier coefficients of type-II plotted as a function of the outgoing frequency x for different choices of μ and μ'. *Left panels* show $\tilde{r}^{(k),0}_{\rm II,H}$ and *right panels* show $\tilde{r}^{(k),0}_{\rm II,F}$. The damping parameter $a = 0.001$. Thin lines correspond to $x' = 1$ and thick lines to $x' = 4$. Solid, dotted, dashed, dot-dashed, and dash-triple-dotted lines correspond to $k = 0, 1, 2, 3$, and 4, respectively. For notational brevity we simply dropped the M dependence on the y-title of the plotted functions.

changes in the converged solution that was obtained when we kept only $k' = 0$ components. This clearly shows that the coupling of k to $k' = 0$ is the dominant one, while the coupling to other $k' \neq 0$ Fourier components is negligible, and if retained, it only increases the dimensionality of the problem (without any increase in accuracy) because of the condition $k' = k + Q' - Q''$. The $\tilde{S}^{(k)2}_{1,Q}$ at order n are given by

$$\left[\tilde{S}^{(k)2}_{1,Q}(\tau, x, \theta)\right]^{(n)} \simeq \left[\tilde{S}^{(k)2}_{1,Q}(\tau, x, \theta)\right]^{(1)} + \sum_{Q'} \frac{1}{2} \int_{-\infty}^{+\infty} \int_0^{\pi} \frac{\tilde{\mathcal{N}}^{(k)2}_{QQ'}(x, \theta, x', \theta', \boldsymbol{B})}{\varphi(x)} \sum_{Q''} \frac{1}{2} \times \tilde{\Gamma}^{(k)}_{2Q',2Q''}(\theta') \left[\tilde{I}^{(0)2}_{Q''}(\tau, x', \theta')\right]^{(n-1)} \sin\theta' \, {\rm d}\theta' \, {\rm d}x', \quad (17)$$

with $k = Q'' - Q'$. Notice that $\left[\tilde{S}^{(k)2}_{1,Q}(\tau, x, \theta)\right]^{(1)}$ are zero for $k = \pm 3$ and ± 4. The explicit forms of $\tilde{\Gamma}^{(k)}_{2Q',2Q''}(\theta)$ are given in Appendix B.

5. Azimuthal Fourier coefficients of magnetic redistribution functions

Extension of the decomposition technique of Frisch (2009) to the Hanle redistribution matrix given by approximation I (see Sect. 2), involves the application of the Fourier azimuthal expansion to the magnetic redistribution functions (see Sect. 3 and Appendix A). For a $J = 0 \rightarrow 1 \rightarrow 0$ scattering transition there are six components of type-II magnetic redistribution functions. They are denoted by $R^{\rm II,X}_{M0}$, where X stands for H (Voigt type) or F (Faraday-Voigt type), and $M = 0, \pm 1$. We denote the corresponding azimuthal Fourier coefficients by $\tilde{r}^{(k),M}_{\rm II,X}$. We note that $\tilde{r}^{(0),M}_{\rm II,H}$ and $\tilde{r}^{(0),M}_{\rm II,F}$ are normalized to the corresponding magnetically shifted Voigt and Faraday-Voigt profile functions. All $k \neq 0$ components are normalized to zero.

The method of computation of azimuthal Fourier coefficients of Hummer's redistribution functions are discussed in detail in Sect. 4 of Sampoorna et al. (2011). The same method has been appropriately extended to compute the azimuthal Fourier coefficients of magnetic redistribution functions. Hence we do not again repeat those details here.

For a weak magnetic field (Hanle $\Gamma = 1$), different M components of type-II function differ very little (graphically indistinguishable). These differences are relevant when the difference of two such components is formed in the composite redistribution functions (see Eq. (A.2)). These difference quantities are responsible for a smooth switch-over from Hanle scattering in the line core to the Rayleigh scattering in the wings. Therefore we show only the azimuthal Fourier coefficients $\tilde{r}^{(k),0}_{\rm II,X}$ for $k = 0, 1, 2, 3$, and 4 in Fig. 2.

From the left panels of Fig. 2 we see that the behavior of $\tilde{r}^{(k),0}_{\rm II,H}$ for $k = 0, 1$, and 2 are identical to those presented in Fig. 2 of Sampoorna et al. (2011). As expected, the $k = 3$ and $k = 4$ components are much smaller than the $k = 0$ component, except for forward and backward scattering (see Figs. 2b and 2c). The function $\tilde{r}^{(k),0}_{\rm II,F}$ takes both positive and negative values not only for $k \neq 0$ but also for $k = 0$, because it involves Faraday-Voigt-type functions. For forward and backward scattering, $\tilde{r}^{(k),0}_{\rm II,H}$ exhibits sharp peaks at $|x| = 1$ when $x' = 1$. On the other hand, for forward scattering the function $\tilde{r}^{(k),0}_{\rm II,F}$ exhibits a zero cross-over at $|x| = 1$ when $x' = 1$ (see Fig. 2e), which is typical of the behavior of Faraday-Voigt functions. However, for backward scattering, $\tilde{r}^{(k),0}_{\rm II,F}$ shown in Fig. 2f does not show a cross-aver at $|x| = 1$. For

$x' = 4$, $\tilde{r}^{(k),0}_{\rm II,F}$ behave similar to the corresponding $\tilde{r}^{(k),0}_{\rm II,H}$ (namely dominance of the frequency coherent nature of type-II function).

6. Results and discussions

We considered isothermal, self-emitting plane-parallel atmospheres with no incident radiation at the boundaries. These slab models are characterized by (T, a, ϵ, r), where T is the optical thickness of the slab. The Planck function at the line center B_{ν_0} is taken as unity. A logarithmic depth grid with five points per decade is used, with the first depth point at $\tau_1 = 10^{-4}$. For the frequency grid we used equally spaced points in the line core and logarithmically spaced ones in the wings. Furthermore, the maximum frequency $x_{\rm max}$ was chosen such that the condition $\varphi(x_{\rm max})T \ll 1$ is satisfied. We have typically 70 points in the interval $[0, x_{\rm max}]$. We used a seven-point Gaussian quadrature in $[0 < \mu \leq 1]$.

6.1. Comparison with the perturbation method

In this section we compare the emergent solutions obtained from the SEM approach for angle-dependent PRD Hanle transfer problem presented in Sect. 4 and the corresponding solution computed from an independent method, namely the perturbation method of Nagendra et al. (2002). We present this comparison for 1D cut-off approximation (Sect. 6.1.1), approximation II (Sect. 6.1.2), and approximation I (Sect. 6.1.3).

We recall that the method presented in Nagendra et al. (2002) solves the polarized transfer equation with angle-dependent PRD and Hanle effect perturbatively in the Stokes vector basis. In this method it is necessary to discretize the azimuth χ of the radiation field apart from the frequency x and orientation θ. As a result, the CPU and memory requirements for this method are pretty high compared to the SEM approach described in the present paper (because in the SEM we do not have to discretize the azimuth χ).

For all figures presented in this section, $a = 10^{-3}$, $\epsilon = 10^{-3}$, $r = 0$ (pure line case), and the line of sight is defined by $\mu = 0.11$ and $\chi = 0°$. The magnetic field parameters are taken as $\Gamma = 1$, $\theta_B = 30°$, and $\chi_B = 0°$. For the perturbation method we used a 16 point trapezoidal grid for $\chi \in [0, 2\pi]$.

6.1.1. 1D frequency cut-off approximation

Here we present the emergent solution computed with a 1D cut-off approximation for the Hanle redistribution matrix (see Sect. 2 for more details). A 1D cut-off frequency with $x_{\rm c} = 3$ Doppler widths was used.

Figure 3 shows the log I, Q/I, and U/I for $T = 1$ (panel (a)), and $T = 10^4$ (panel (b)). The solid line shows the multiple scattered solution from the SEM approach, and the dashed line shows the corresponding multiple scattered solution from the perturbation method. The single scattered solution is shown as a dotted line for comparison. Spikes or dents observed around $x = 3$ are caused by the abrupt cut-off used. Clearly, the multiple scattered solution from the SEM approach compares fairly well with the corresponding solution from the perturbation method. The slight differences noticed around the line center are caused by the finite resolution of the azimuth angle grid used in the perturbation method (with 16 points). We have verified that these differences decrease when we increase the number of azimuth points from 16 to 36, but at the cost of huge memory and CPU time. In the SEM approach the transfer problem is solved on a basis of azimuth-independent (reduced) Fourier coefficients. The azimuth dependence is finally recovered when transforming into the Stokes vector basis (see our Eq. (10), and Eqs. (B.1)–(B.3) of Frisch 2007).

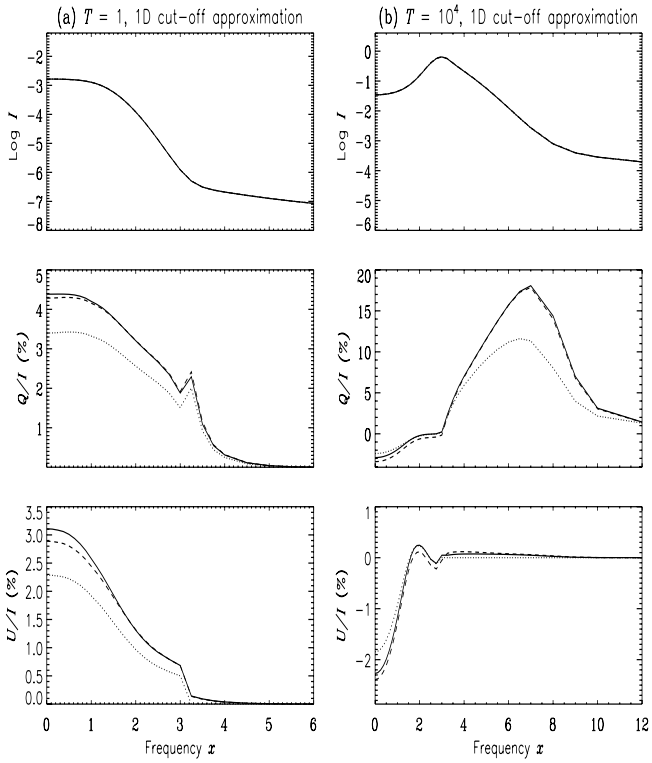

Fig. 3. Comparison of the multiple scattered solution from the SEM (solid lines) and of that from the perturbation method (dashed lines). Dotted lines represent the single scattered solution. The 1D cut-off approximation is used with $x_{\rm c} = 3$. The model parameters are (a, ϵ, r) = (10^{-3}, 10^{-3}, 0) and the magnetic field parameters are (Γ, θ_B, χ_B) = (1, 30°, 0°). The line of sight is represented by $\mu = 0.11$ and $\chi = 0°$. Panel **a)** corresponds to $T = 1$ and panel **b)** to $T = 10^4$. The positive Q direction corresponds to the linear polarization perpendicular to the solar limb.

6.1.2. 2D frequency domains

Here we present the solutions computed using the domain-based Hanle scattering redistribution matrix (approximation II) discussed in Sect. 2. Figure 4 shows the emergent solutions for $T = 1$ (panel (a)), and $T = 10^4$ (panel (b)). The solid lines again represent the multiple scattered solution from SEM approach, and the dashed lines represent the corresponding solution from the perturbation method. We recall that angle-averaged frequency domains of approximation III with angle-dependent PRD functions are used in the SEM approach, while the actual approximation II (angle-dependent frequency domains) of Bommier (1997) is used in the perturbation method.

As for the 1D cut-off approximation, the differences observed near the line center between the multiple scattered solution from the SEM approach and the perturbation method are caused by the finite resolution of the χ grid in the perturbation method. However, considerable differences are observed between the two solutions in the transition region $3 \leq x \leq 4$. These differences are not caused by the finite resolution of the χ grid in the perturbation method. But they are caused by the use of angle-averaged frequency domains to solve the angle-dependent PRD

Table 1. CPU time requirements for the SEM approach proposed in this paper and the perturbation method of Nagendra et al. (2002) for different values of optical thickness T.

Optical thickness T	SEM approach (CPU time in min)	Perturbation method (CPU time in min)
1	10	36
10	95	275
100	110	413
10^3	101	448
10^4	112	532

Notes. The PRD function computation times are excluded from the CPU time given in this table, because they are common to both the methods. The model parameters and the grid specifications are the same as those discussed in Sect. 6.1. The computations were performed on a Sun Fire V20z Server, 2385 MHz, with a single-core AMD Opteron processor.

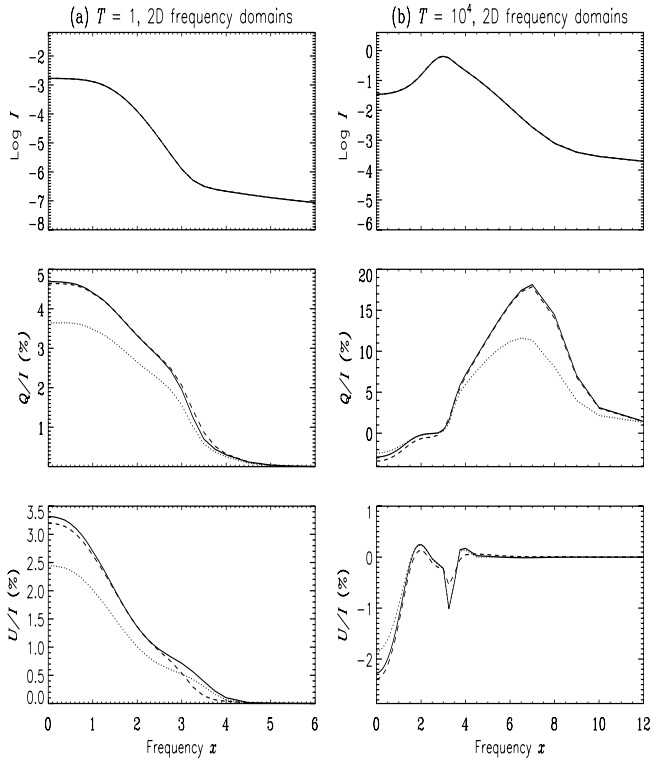

Fig. 4. Same as Fig. 3, but with 2D frequency domains of Bommier (1997) in the Hanle PRD matrix.

transfer problem in the SEM approach. However, there seems to be no way to include self-consistently the angle-dependent frequency domains explicitly in the SEM approach. Our attempts to derive azimuth-averaged frequency domains were not successful, and still remain an open theoretical problem. Nevertheless, the SEM approach is shown to be numerically superior to the perturbation method, as can be seen from Table 1.

In Table 1 we compare the CPU time requirements for SEM and perturbation method for $T = 1$, 10, 100, 10^3, and 10^4. From Table 1 we see that the SEM approach is faster than the perturbation approach, particularly for slabs of larger optical thickness T. This is because as T increases, the perturbation method converges slowly, because it is basically a classical lambda iteration on Stokes source vector components S_Q and S_U, and actually fails to converge for higher values of T, whereas the SEM approach works for any value of T and for any choice of the

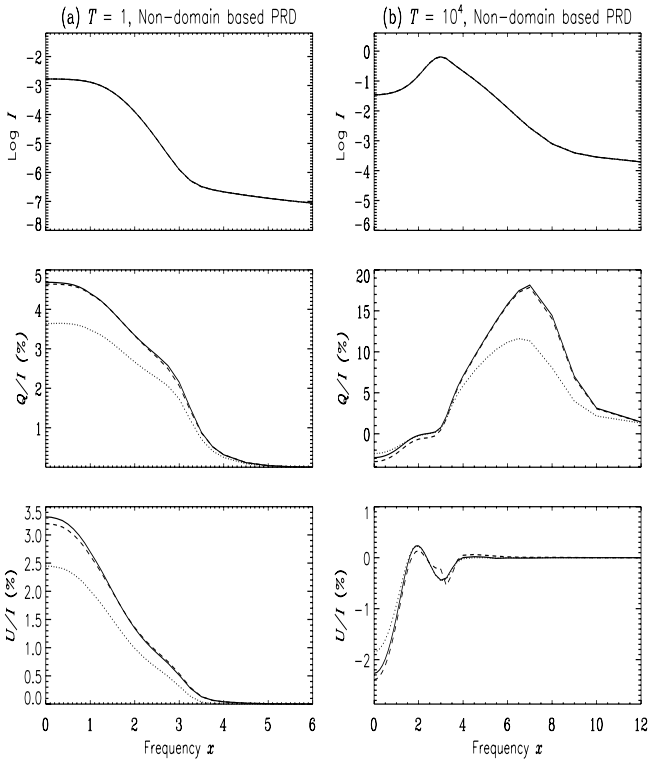

Fig. 5. Comparison of the multiple scattered solution from the SEM (solid lines) and that from the perturbation method (dashed lines). Dotted lines represent the single scattered solution. Approximation I (non-domain-based PRD) is used for the SEM approach, while approximation II (2D angle-dependent frequency domains) is used in the perturbation method. Other model parameters are the same as in Fig. 3.

model parameters. Because the starting solution, namely the single scattered solution, is already a good approximation to the full solution (compare solid and dotted lines in Figs. 3–5), the SEM converges faster and thereby requires less CPU time. Moreover, the SEM approach requires about 1 GB of main memory, while the perturbation method requires about 11 GB for the same line transfer problem.

6.1.3. Non-domain-based PRD theory

Figure 5 shows a comparison between the emergent solutions computed using approximation I (non-domain-based PRD) in the SEM approach (solid lines) and the approximation II (domain-based PRD) in the perturbation method (dashed lines). For thin slabs (panel (a)) both solutions match at all the frequencies, except near the line center, which as before is caused by the finite resolution of the χ grid in the perturbation method. For thicker slabs (panel (b)) we note that Q/I is nearly insensitive to the frequency space decomposition, while U/I shows some difference particularly at the transition region $3 \leq x < 4$. The non-domain-based PRD theory produces smoother U/I profiles at all frequencies, while the domain-based PRD theory produces sharp peaks at the transition region between the line core and line wings owing to abrupt cut-offs.

6.2. Hanle Stokes profiles computed with angle-dependent and angle-averaged non-domain-based PRD matrix

Following Sampoorna et al. (2011, see however Sect. 8 of the present paper for an erratum to that paper), here we present a

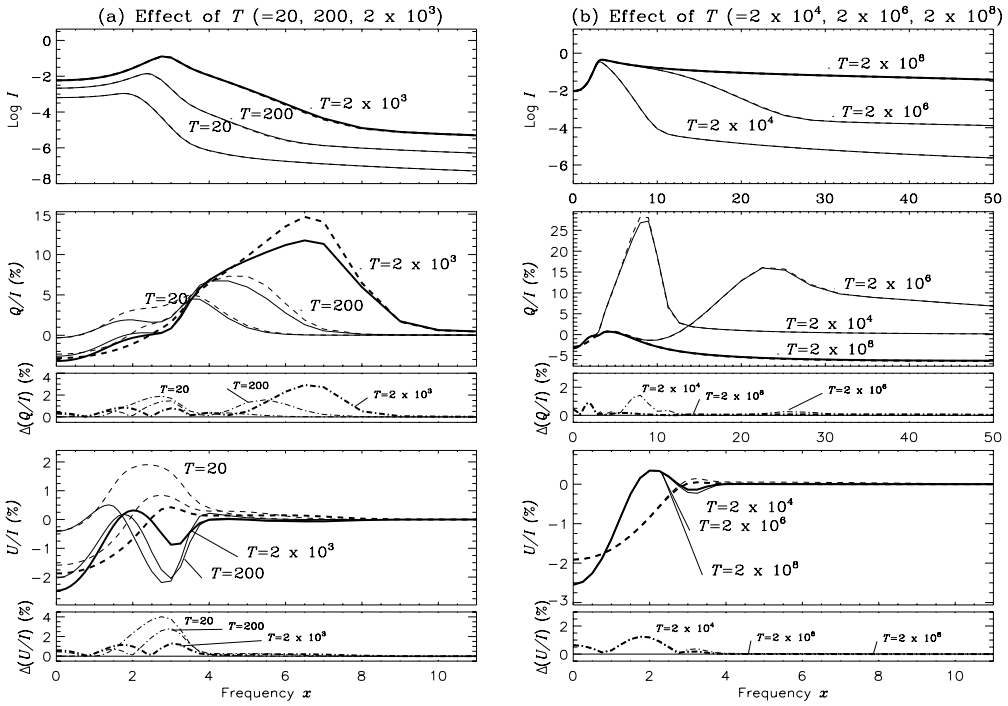

Fig. 6. The emergent I, Q/I, and U/I profiles at $\mu = 0.11$ and $\chi = 0°$ computed for the angle-averaged (dashed lines) and the angle-dependent (solid lines) non-domain-based PRD. Panel **a)**: thin lines $T = 20$, medium thick lines $T = 200$, and thick lines $T = 2 \times 10^3$. Panel **b)**: thin lines $T = 2 \times 10^4$, medium thick lines $T = 2 \times 10^6$, and thick lines $T = 2 \times 10^8$. Other model parameters are $(a, \epsilon, r) = (10^{-3}, 10^{-4}, 0)$. The absolute differences $\Delta(Q/I)$ and $\Delta(U/I)$ in percentage are also shown.

comparison of emergent Hanle Stokes profiles computed with angle-dependent and angle-averaged PRD functions for several atmospheric parameters. For this purpose we consider the non-domain-based PRD matrix (approximation I) of Bommier (1997). The angle-averaged version of this PRD matrix has been implemented in a polarized ALI code in Sampoorna et al. (2008). We used this code to compute the angle-averaged solutions, while the corresponding angle-dependent solutions were computed using the SEM approach presented in this paper.

For a study of the differences between angle-dependent and angle-averaged emergent solutions, we consider a standard atmospheric model $(T, a, \epsilon, r) = (2 \times 10^3, 10^{-3}, 10^{-4}, 0)$ around which we vary the various atmospheric parameters one at a time, keeping other parameters fixed. For all figures presented in this section the magnetic field parameters are $(\Gamma, \theta_B, \chi_B) = (1, 30°, 0°)$. Furthermore, in all figures of this section the solid lines represent the angle-dependent solutions and the dashed lines represent the corresponding angle-averaged solutions.

6.2.1. Effect of optical thickness T

In Fig. 6 we compare the emergent I, Q/I, and U/I profiles computed with angle-averaged (dashed lines) and the angle-dependent (solid lines) non-domain-based PRD matrix for different values of optical thickness T. We cover a range of optical thickness from thin slabs ($T = 20$) to very thick slabs ($T = 2 \times 10^8$). Below each of the Q/I and U/I panels we also plot the absolute difference $\Delta(X/I) = |(X/I)_{\rm AD} - (X/I)_{\rm AA}|$ in percentage, where X stands for Q or U and the acronyms AD for angle-dependent and AA for angle-averaged.

As the optical thickness T increases, the amplitude of the near wing peak in Q/I initially increases until $T = 2 \times 10^4$. For $T > 2 \times 10^4$ the near wing peak amplitude decreases. This trend is also followed by the absolute difference $\Delta(Q/I)$. The biggest differences are noted for $T = 2 \times 10^3$, however. The U/I profiles on the other hand show considerable differences in their shapes themselves for all values of T. Only for $T = 20$ the angle-dependent and angle-averaged solutions match near the line center. For other values of T differences are observed for all frequencies in the range $0 \le x \le 5$. The absolute difference $\Delta(U/I)$ is most pronounced for $T = 20$. Consequently, angle-dependent PRD effects are more important for U/I profiles than for Q/I profiles.

It is interesting to note that the U/I profiles for $T \ge 2 \times 10^4$ are all identical. Moreover, the intensity I and Q/I in the line core are nearly the same for these optical thicknesses. This behavior can perhaps be explained with the concept of thermalization depths and thermalization frequencies (Frisch 1980). The thermalization depth $\tau_{\rm th}$ defines the depth below which the source function for Stokes I departs from the Planck function, and above which the source function is equal to the Planck function. The thermalization frequency $x_{\rm th}$ defines the frequency below which the source function equals the Planck function for $\tau > \tau_{\rm th}$, and above which the source function departs from the Planck function at all depths. In the case of angle-averaged type-II redistribution function of Hummer (1962), Frisch (1980) and Hubený (1985) show that the thermalization depth and thermalization frequency in the line core are $x^c_{\rm th} = a^{1/3}\epsilon^{-1/3}$ and $\tau^c_{\rm th} = 1/\epsilon$, while in the line wings they are $x^w_{\rm th} = 1/\sqrt{\epsilon}$ and $\tau^w_{\rm th} = 1/(a\epsilon^{3/2})$, respectively. For $a = 10^{-3}$ and $\epsilon = 10^{-4}$ we have $x^c_{\rm th} = 2.15$, $\tau^c_{\rm th} = 10^4$, $x^w_{\rm th} = 100$, and $\tau^w_{\rm th} = 10^9$. Clearly, all photons with frequencies $x \le x^c_{\rm th}$ are thermalized for $T \ge 2 \times 10^4$, which explains the observed behavior of I, Q/I, and U/I at these frequencies.

6.2.2. Effects of the thermalization parameter ϵ and the continuum strength parameter r

Figure 7a shows the effect of ϵ on the difference between the angle-dependent and angle-averaged emergent solutions.

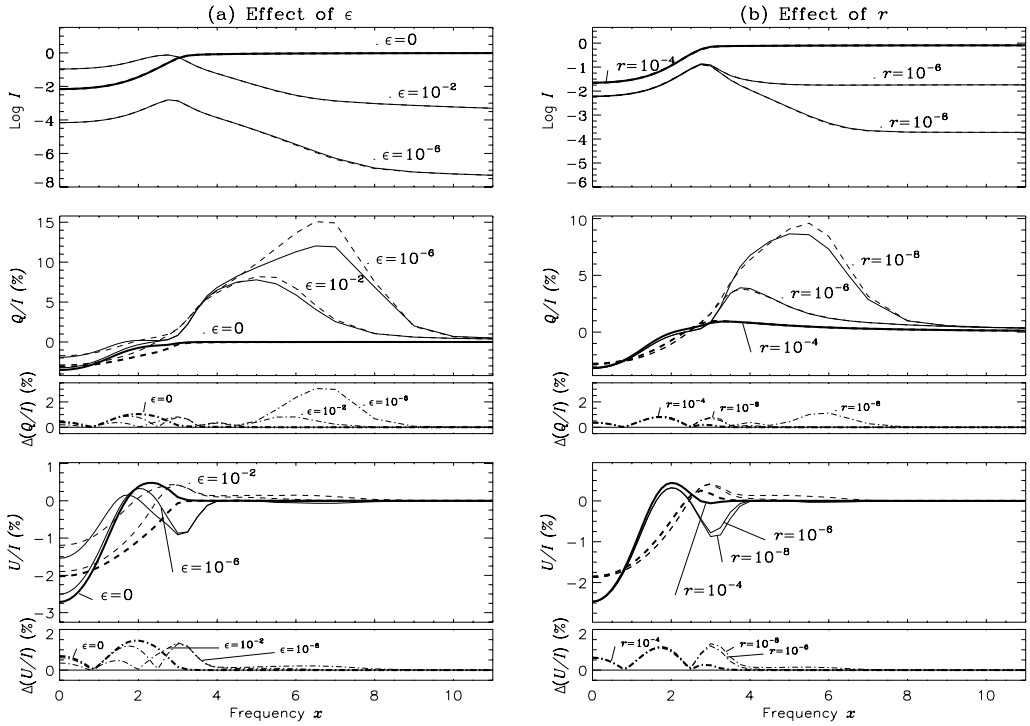

Fig. 7. The emergent I, Q/I, and U/I profiles at $\mu = 0.11$ and $\chi = 0°$ computed for the angle-averaged (dashed lines) and the angle-dependent (solid lines) non-domain-based PRD. Panel **a)**: thin lines $\epsilon = 10^{-2}$, medium thick lines $\epsilon = 10^{-6}$, and thick lines $\epsilon = 0$. Panel **b)**: thin lines $r = 10^{-8}$, medium thick lines $r = 10^{-6}$, and thick lines $r = 10^{-4}$. Other model parameters are $(T, a) = (2 \times 10^3,\ 10^{-3})$. For panel **a)** $r = 0$, and for panel **b)** $\epsilon = 10^{-4}$. The absolute differences $\Delta(Q/I)$ and $\Delta(U/I)$ in percentage are also shown.

As expected, the intensity I increases with an increase in ϵ, while the degree of polarization (both Q/I and U/I) decreases. The differences between Q/I profiles computed with the angle-dependent and angle-averaged PRD essentially decrease at all frequencies as ϵ increases from 10^{-6} to 10^{-2}. But for the U/I profiles the differences decrease for $|x| \leq 3$, beyond which the differences are the same for both $\epsilon = 10^{-6}$ and 10^{-2}. In the same figure we also show the case of conservative scattering ($\epsilon = 0$). Here an unpolarized incident radiation is given as the lower boundary condition, namely, $\tilde{I}_Q^{(k)K}(\tau = T, x, \theta) = \delta_{0k}\delta_{K0}\delta_{Q0}2B_{\nu_0}$, because there is no primary source of photons. The emergent Q/I and U/I are confined to the line core ($|x| \leq 3$), where we observe some differences between the angle-dependent and angle-averaged cases.

The effect of the continuum strength parameter r on the differences between angle-dependent and angle-averaged profiles is shown in Fig. 7b. As in the non-magnetic case (see Fig. 11 of Sampoorna et al. 2011), there is a gradual decrease of the differences between angle-dependent and angle-averaged Q/I profiles with an increase in r, particularly at the near wing maxima. The U/I profiles on the other hand show only a small sensitivity to r in the frequency range $2 < x < 5$, where the differences also decrease with an increase in r.

6.2.3. Center-to-limb variations

As in Sampoorna et al. (2011), we show in Fig. 8 the center-to-limb variation of the emergent I, Q/I, and U/I profiles and also of the difference between angle-dependent and angle-averaged polarization profiles. Clearly as $\mu \to 1$ the absolute differences in both Q/I and U/I tend to zero. However, there are significant differences in the shapes of the U/I profiles computed with angle-dependent and angle-averaged PRD. Also the magnitude of Q/I profiles computed with angle-dependent PRD is smaller than those computed with angle-averaged PRD, while the opposite is the case for U/I profiles. It is interesting to note that the amplitude of the minima in angle-dependent U/I at $x = 3$ seems to increase as μ changes from 0.7 to 0.97.

7. Conclusions

We have developed an iterative method based on the Neumann series expansion of the polarized source vector components to solve the complex transfer problem with angle-dependent PRD and Hanle effect. This method, originally developed by Frisch et al. (2009) for CRD problems, was generalized to the angle-dependent PRD non-magnetic transfer problems by Sampoorna et al. (2011), who referred to it as the scattering expansion method (SEM). Thanks to the decomposition method developed by Frisch (2009), we were able to formulate here an efficient iterative method to solve this complex problem. In this method, the polarized radiation field is first decomposed into six irreducible components, which remain non-axisymmetric because of the use of angle-dependent PRD function, however. These non-axisymmetric components are then reduced to $6 \times (2n_k - 1)$ Fourier components using a Fourier azimuthal expansion of the angle-dependent PRD function (where n_k is the number of positive k values including zero). Clearly, one obtains an infinite set of integral equations for the Fourier components of the irreducible source vector because k in general takes values from $-\infty$ to $+\infty$. Sampoorna (2011b) showed that the number of Fourier components can be limited to 26 when one applies the single scattering approximation (see e.g., Frisch et al. 2009). This is because the value of k is limited to $k = 0, \pm 1, \pm 2$ in this case. The single scattering approximation gives a reasonable approximation to the full solution. We showed how to include higher-order

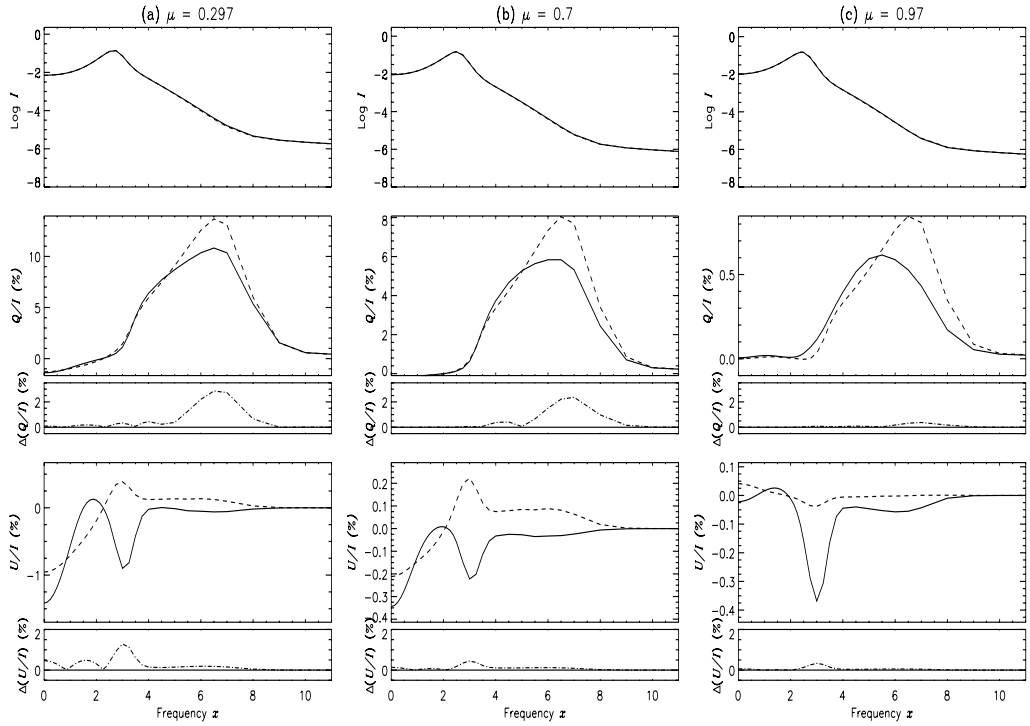

Fig. 8. The emergent I, Q/I, and U/I profiles for different values of the heliocentric angle computed for the angle-averaged (dashed lines) and the angle-dependent (solid lines) non-domain-based PRD. The atmospheric model used is $(T, a, \epsilon, r) = (2\times10^3, 10^{-3}, 10^{-4}, 0)$. The absolute differences $\Delta(Q/I)$ and $\Delta(U/I)$ in percentage are also shown.

terms to develop the SEM approach as a solution technique. Including higher-order terms increases the number of Fourier components to 46 because k now takes values $0, \pm1, \pm2, \pm3$, and ±4. For the Hanle scattering redistribution matrix, we have considered both the exact (approximation I of Bommier 1997) and approximate (approximation II of Bommier 1997, 1D cut-off approximation) forms. We confined our attention only to pure type-II scattering.

We have shown that the SEM approach is computationally more efficient (see Table 1) than the perturbation method of Nagendra et al. (2002). When a 1D cut-off approximation is used for the Hanle redistribution matrix, both the SEM approach and the perturbation method give nearly the same solutions. However, the differences between the solutions obtained from both the methods occur near the transition region $3 \le x \le 4$, when the approximation II of Bommier (1997) is used. The reason is that in the SEM approach angle-averaged frequency domains are used for handling the angle-dependent transfer problem, while actual angle-dependent frequency domains are used in the perturbation method. Because the SEM approach is devised based on azimuthally symmetric Fourier components, the actual angle-dependent frequency domains cannot be implemented in this approach. It needs the derivation of azimuth-averaged frequency domains, which is beyond the scope of the present paper. In spite of this difficulty, we have shown that SEM approach is still able to handle angle-dependent transfer using angle-averaged frequency domains to a sufficient accuracy. Furthermore, the SEM approach can handle slabs of any optical thickness, while the older perturbation method suffers from convergence problems for thick slabs because it essentially is a method based on classical lambda iteration on the linear polarization components of the source vector.

We have carried out a detailed numerical study to analyze the role of angle-dependent PRD effects. For this purpose we have used the angle-dependent and angle-averaged versions of the non-domain-based PRD matrices (approximation I) of Bommier (1997). In the presence of a weak magnetic field the Q/I profiles computed with angle-dependent and angle-averaged PRD show significant differences both around the line core and near wing maxima for $T \le 2\times10^3$. For $T \ge 2\times10^4$ the differences are small and appear mainly near the line core. The U/I profiles on the other hand show significant differences in the shape itself at all optical depths and almost at all frequencies. Therefore we reconfirm the conclusions of Nagendra et al. (2002) that the U/I profiles are highly sensitive to the angle-dependence of the PRD function, and should be taken into account for magnetic field determination based on Hanle effect.

8. Erratum

Figures 6–8 and Figs. 10–12 of Sampoorna et al. (2011) are slightly erratic, and consequently the conclusions drawn based on them. These figures show the comparison of the non-magnetic Stokes Q and Q/I profiles computed with angle-dependent (solid lines) and angle-averaged (dashed lines) PRD functions. The error lies in the fact that these comparisons were not made on the same footing. The angle-averaged functions in Sampoorna et al. (2011) were computed using the method described in Gouttebroze (1986) combined with the frequency grid refinement discussed in Sect. 4 of Sampoorna et al. (2011). In the present paper we calculated the angle-averaged PRD functions by explicitly angle-averaging the corresponding angle-dependent PRD functions (see Eqs. (103) and (104) of Bommier 1997), using a 31-point Gauss-Legendre quadrature. This method of computing the angle-averaged PRD function is also combined with the frequency grid refinement discussed in Sect. 4 of Sampoorna et al. (2011). We found that these two different methods of computing the same angle-averaged function give slightly different emergent Stokes Q profiles. This in turn affects the difference between the Q/I profiles computed with the angle-dependent and angle-averaged PRD functions.

We note that Stokes I is not much affected by any of the two methods used for computing angle-averaged PRD function.

We think that computing the angle-averaged functions by explicit angle-averaging is on par with the computation of corresponding angle-dependent functions because the error made (if any) in the computation will be on a similar order. Consequently, only one conclusion of Sampoorna et al. (2011, see last two sentences in their abstract and first two sentences of last but one paragraph of their conclusions section) is incorrect. Instead that conclusion should read as follows: the relative difference in the emergent polarization rate Q/I computed with angle-dependent and angle-averaged PRD functions is between 10% and 30% for slabs with optical thickness $20 \le T \le 2 \times 10^3$, the largest differences occurring in the near wing peaks. For slabs of optical thickness $T \ge 2 \times 10^4$ the differences are comparatively smaller (and occur only around the line core) and therefore angle-averaged PRD functions can safely be used. These conclusions now agree with the conclusions of the present paper and those of Nagendra et al. (2002) and Faurobert (1987, 1988).

Appendix A: Composite redistribution functions of type-II

The composite redistribution function of type-II, $\mathcal{R}^{K,K}_{Q,\mathrm{II}}(x, x', \Theta, B)$ are obtained after applying the Doppler broadening to the rest frame quantity $\delta(\nu - \nu')\Phi^{K,K}_Q(J, J'; \nu')$ of Bommier (1997, see her Eq. (81)), where $\Phi^{K,K}_Q(J, J'; \nu')$ are generalized profile functions (see Landi Degl'Innocenti et al. 1991). For a $J \to J' \to J$ scattering transition, it takes the form

$$\mathcal{R}^{K,K}_{Q,\mathrm{II}}(x, x', \Theta, B) = \sqrt{3(2J'+1)}(2K+1) \sum_{MM'Npp'} (-1)^{J'-N-1+Q} \begin{pmatrix} J' & K & J' \\ -M & Q & M' \end{pmatrix} \times \begin{pmatrix} J & 1 & J' \\ -N & -p & M \end{pmatrix} \begin{pmatrix} J & 1 & J' \\ -N & -p' & M' \end{pmatrix} \begin{pmatrix} 1 & 1 & K \\ -p & p' & Q \end{pmatrix} \times \frac{1}{2}\left[R^{\mathrm{II,H}}_{MN} + R^{\mathrm{II,H}}_{M'N} + \mathrm{i}\left(R^{\mathrm{II,F}}_{M'N} - R^{\mathrm{II,F}}_{MN}\right)\right], \quad (A.1)$$

where M, M' and N denote the magnetic substates of the upper level J' and the lower level J, respectively. The magnetic redistribution functions $R^{\mathrm{II,H}}_{MN}$ and $R^{\mathrm{II,F}}_{MN}$ are defined in Eqs. (24)–(26) of Sampoorna (2011a), but with the energy conservation term $x_{NN''}$ set to zero because it is neglected in approximation I (see Sect. 4.1 of Bommier 1997). Here "H" stands for Voigt type and "F" for Faraday-Voigt type functions.

In the present paper we considered only a $J = 0 \to 1 \to 0$ scattering transition. In this case the explicit form of $\mathcal{R}^{K,K}_{Q,\mathrm{II}}$ are listed in Appendix A of Sampoorna et al. (2007b), where it is denoted by the symbol $\Phi^{K,K}_{Q,\mathrm{II}}$. For easy reference we list them here in a slightly different form (namely, M, M' here corresponds to $-q$ and $-q'$ of Sampoorna et al. 2007b).

$$\begin{aligned}
\mathcal{R}^{0,0}_{0,\mathrm{II}} &= \frac{1}{3}\left(R^{\mathrm{II,H}}_{10} + R^{\mathrm{II,H}}_{00} + R^{\mathrm{II,H}}_{-10}\right), \\
\mathcal{R}^{2,2}_{0,\mathrm{II}} &= \frac{1}{6}\left(R^{\mathrm{II,H}}_{10} + R^{\mathrm{II,H}}_{-10}\right) + \frac{2}{3}R^{\mathrm{II,H}}_{00}, \\
\mathcal{R}^{2,2}_{1,\mathrm{II}} &= \frac{1}{4}\left[R^{\mathrm{II,H}}_{10} + 2R^{\mathrm{II,H}}_{00} + R^{\mathrm{II,H}}_{-10} + \mathrm{i}\left(R^{\mathrm{II,F}}_{-10} - R^{\mathrm{II,F}}_{10}\right)\right], \\
\mathcal{R}^{2,2}_{2,\mathrm{II}} &= \frac{1}{2}\left[R^{\mathrm{II,H}}_{10} + R^{\mathrm{II,H}}_{-10} + \mathrm{i}\left(R^{\mathrm{II,F}}_{-10} - R^{\mathrm{II,F}}_{10}\right)\right], \\
\mathcal{R}^{2,2}_{-Q,\mathrm{II}} &= \left(\mathcal{R}^{2,2}_{Q,\mathrm{II}}\right)^*, \quad \text{for } Q = 1, 2. \quad (A.2)
\end{aligned}$$

Appendix B: The azimuthal Fourier coefficients $\tilde{\Gamma}^{(Q'-Q)}_{KQ,K'Q'}$

The azimuthal Fourier coefficients $\tilde{\Gamma}^{(Q'-Q)}_{KQ,K'Q'}$ are defined in Eq. (12). It is easy to verify that they satisfy the following properties

$$\left[\tilde{\Gamma}^{(Q'-Q)}_{KQ,K'Q'}\right]^* = \tilde{\Gamma}^{(Q-Q')}_{K'Q',KQ}, \quad (B.1)$$

$$\tilde{\Gamma}^{(Q-Q')}_{K-Q,K'-Q'} = (-1)^{Q+Q'}\left[\tilde{\Gamma}^{(Q'-Q)}_{KQ,K'Q'}\right]^*. \quad (B.2)$$

Owing to the above-mentioned symmetry relations, there are only 13 independent coefficients. For $i = 0, 1$ and the reference angle $\gamma = 0$ (see Landi Degl'Innocenti & Landolfi 2004), the form of $\tilde{\mathcal{T}}^K_Q(i, \mu)$ are given in Eq. (A.6) of Frisch (2010). For $i = 2$ and the reference angle $\gamma = 0$, $\tilde{\mathcal{T}}^K_Q(i, \mu)$ are given by

$$\begin{aligned}
&\tilde{\mathcal{T}}^0_0(2, \mu) = 0; \qquad \tilde{\mathcal{T}}^2_0(2, \mu) = 0, \\
&\tilde{\mathcal{T}}^2_1(2, \mu) = -\mathrm{i}\frac{\sqrt{3}}{2}\sqrt{1-\mu^2}; \quad \tilde{\mathcal{T}}^2_2(2, \mu) = -\mathrm{i}\frac{\sqrt{3}}{2}\mu. \quad (B.3)
\end{aligned}$$

Using Eq. (A.6) of Frisch (2010) and our Eq. (B.3) in Eq. (12), we obtain the following explicit form for these coefficients:

$$\begin{aligned}
&\tilde{\Gamma}^{(0)}_{00,00} = 1; \quad \tilde{\Gamma}^{(0)}_{20,00} = \frac{1}{2\sqrt{2}}(3\mu^2 - 1), \\
&\tilde{\Gamma}^{(1)}_{2-1,00} = \frac{\sqrt{3}}{2}\mu\sqrt{1-\mu^2}; \quad \tilde{\Gamma}^{(2)}_{2-2,00} = \frac{\sqrt{3}}{4}(1-\mu^2), \\
&\tilde{\Gamma}^{(0)}_{20,20} = \frac{1}{4}(9\mu^4 - 12\mu^2 + 5), \\
&\tilde{\Gamma}^{(1)}_{20,21} = \frac{\sqrt{3}}{2\sqrt{2}}\mu\sqrt{1-\mu^2}(2 - 3\mu^2), \\
&\tilde{\Gamma}^{(2)}_{20,22} = \frac{\sqrt{3}}{4\sqrt{2}}(1-\mu^2)(1+3\mu^2), \\
&\tilde{\Gamma}^{(0)}_{21,21} = \frac{3}{4}(1-\mu^2)(1+2\mu^2), \\
&\tilde{\Gamma}^{(-2)}_{21,2-1} = \frac{3}{4}(1-\mu^2)(1-2\mu^2), \\
&\tilde{\Gamma}^{(1)}_{21,22} = \frac{3}{4}\mu\sqrt{1-\mu^2}(1+\mu^2), \\
&\tilde{\Gamma}^{(-3)}_{21,2-2} = -\frac{3}{4}\mu\sqrt{1-\mu^2}(1-\mu^2), \\
&\tilde{\Gamma}^{(0)}_{22,22} = \frac{3}{8}(1+\mu^2)^2; \quad \tilde{\Gamma}^{(-4)}_{22,2-2} = \frac{3}{8}(1-\mu^2)^2. \quad (B.4)
\end{aligned}$$

References

Anusha, L. S., & Nagendra, K. N. 2011, ApJ, 739, 40
Anusha, L. S., Nagendra, K. N., Bianda, M., et al. 2011, ApJ, 737, 95
Bommier, V. 1997, A&A, 328, 726
Chandrasekhar, S. 1950, Radiative transfer (Oxford: Clarendon Press)
Domke, H., & Hubeny, I. 1988, ApJ, 334, 527
Faurobert, M. 1987, A&A, 178, 269
Faurobert, M. 1988, A&A, 194, 268
Faurobert-Scholl, M. 1992, A&A, 258, 521
Fluri, D. M., Nagendra, K. N., & Frisch, H. 2003, A&A, 400, 303
Frisch, H. 1980, A&A, 83, 166
Frisch, H. 2007, A&A, 476, 665
Frisch, H. 2009, in Solar Polarization 5, ed. S. V. Berdyugina, K. N. Nagendra, & R. Ramelli (San Francisco: ASP), ASP Conf. Ser., 405, 87
Frisch, H. 2010, A&A, 522, A41

Frisch, H., Anusha, L. S., Sampoorna, M., & Nagendra, K. N. 2009, A&A, 501, 335
Gouttebroze, P. 1986, A&A, 160, 195
Hamilton, D. R. 1947, ApJ, 106, 457
Hubený, I. 1985, A&A, 145, 461
Hummer, D. G. 1962, MNRAS, 125, 21
Landi Degl'Innocenti, E. 1984, Sol. Phys., 91, 1
Landi Degl'Innocenti, M., & Landi Degl'Innocenti, E. 1988, A&A, 192, 374
Landi Degl'Innocenti, E., & Landolfi, M. 2004, Polarization in Spectral Lines (Dordrecht: Kluwer)
Landi Degl'Innocenti, E., Bommier, V., & Sahal-Bréchot, S. 1991, A&A, 244, 391
Nagendra, K. N., Paletou, F., Frisch, H., & Faurobert-Scholl, M. 1999, in Solar Polarization, ed. K. N. Nagendra, & J. O. Stenflo (Boston: Kluwer), 127
Nagendra, K. N., Frisch, H., & Faurobert, M. 2002, A&A, 395, 305
Nagendra, K. N., Frisch, H., & Fluri, D. M. 2003, in Solar Polarization, ed. J. Trujillo Bueno, & J. Sanchez Almeida (San Francisco: ASP), ASP Conf. Ser., 307, 227
Omont, A., Smith, E. W., & Cooper, J. 1973, ApJ, 182, 283
Sampoorna, M. 2011a, ApJ, 731, 114
Sampoorna, M. 2011b, A&A, 532, A52
Sampoorna, M., Nagendra, K. N., & Stenflo, J. O. 2007a, ApJ, 663, 625
Sampoorna, M., Nagendra, K. N., & Stenflo, J. O. 2007b, ApJ, 670, 1485
Sampoorna, M., Nagendra, K. N., & Frisch, H. 2008, J. Quant. Spec. Radiat. Transf., 109, 2349
Sampoorna, M., Nagendra, K. N., & Frisch, H. 2011, A&A, 527, A89
Stenflo, J. O. 1978, A&A, 66, 241